

Mitigating Source and Detection Noises in Auto-correlative Weak-Value Amplification

Xiang-Yun Hu^{1,*}, Jing-Hui Huang^{1,2,†}, Fei-Fan He⁴, Guang-Jun Wang⁵, and Adetunmise C. Dada^{3,‡}

¹*Hubei Subsurface Multiscale Image Key Laboratory, School of Geophysics and Geomatics, China University of Geosciences, Lumo Road 388, 430074 Wuhan, China.*

²*Department of Physics and Centre for Research in Photonics, University of Ottawa, 25 Templeton Street, Ottawa, Ontario, Canada K1N 6N5*

³*School of Physics and Astronomy, University of Glasgow, Glasgow G12 8QQ, UK*

⁴*Institute of Optics and Electronics, Key Laboratory of Science and Technology on Space Optoelectronic Precision Measurement, Chinese Academy of Sciences, Chengdu 610209, China*

⁵*School of Automation, China University of Geosciences, Lumo Road 388, 430074 Wuhan, China.*

Weak-value amplification (WVA), a post-selection-based technique that amplifies weak physical signals by preparing nearly orthogonal pre- and post-selected quantum states, is intrinsically limited by various kinds of technical noise, which distorts amplified weak values, especially when discarding photons in post-selection. While prior work established the efficacy of auto-correlative weak-value amplification (AWVA) under Gaussian noise, practical implementations face challenges from band-limited laser-source noise and detection noise (including shot noise and electrical noise). Here, we demonstrate that the AWVA protocol robustly suppresses both laser-power fluctuations and detection noise. Numerical experiments in Simulink further reveal AWVA’s dual advantage: under high-power conditions, the noise-reduction superiority of AWVA over WVA becomes increasingly pronounced as input laser power increases, whereas in detection-limited regimes AWVA achieves an order-of-magnitude lower uncertainty, closely approaching the Cramér–Rao bound. Crucially, this work demonstrates that AWVA improves precision in both high-power (laser-noise-dominated) and photon-starved (detector-noise-dominated) regimes, thereby bridging these operating extremes and advancing precision in applications from gravitational-wave detection to hybrid quantum systems.

I. INTRODUCTION

Environmental noise fundamentally limits the precision of quantum measurements [1–5], from probing nanoscale spin dynamics to detecting gravitational waves [6–10]. While weak-value amplification (WVA) [11] enhances parameter estimation by amplifying small signals through post-selection, its sensitivity to noise—particularly non-Gaussian and spectrally structured disturbances—remains a critical challenge [12–19]. This limitation is acute in real-world scenarios, such as optomechanical sensing [20] and gravitational-wave interferometry [6], where band-limited laser source noise and detection noise dominate.

Weak-value amplification leverages post-selection between nearly orthogonal quantum states to generate anomalously large weak values, enabling parameter estimation beyond the bounds of projective measurement [12]. This counterintuitive feature has revolutionized ultrasensitive metrology, achieving transverse optical deflections [21], velocities [22, 23], angular rotation shifts [24, 25], single-photon nonlinearity [26, 27], temperature [28, 29], the weak magnetic fields detection [30], photonic spin hall effect [31–34], frequency shifts [35, 36]. Although postselection discards most photons, an increasing number of experiments and theories have demonstrated the WVA technique [37–40]

and its modifications [14, 23, 41–47] outperform conventional interferometers under specific technical noise conditions. In particular, Amir Feizpour *et al.* demonstrated that WVA can achieve higher SNRs in the presence of low-frequency noise (e.g. 1/f noise) when amplifying single-photon nonlinearity [26]. A recent experiment [48] showed that implementing WVA inside an interferometer can enhance precision, with the signal-to-noise ratio (SNR) approaching the Cramér–Rao bound (CRB). The CRB sets the minimum achievable standard deviation for estimating an unknown parameter, as determined by the statistics of the measured pointer [23, 37, 49–52].

Auto-correlative weak-value amplification (AWVA) suppresses Gaussian noise by correlating time-delayed measurement outcomes, as demonstrated in idealized settings [54]. However, practical quantum and interferometric systems face non-Gaussian noise with distinct spectral and physical origins—band-limited laser-source noise and various detection noise that limit real-world applicability [55–58]. Whereas Ref. [54] considered only additive Gaussian noise, the present work extends AWVA to *band-limited* laser noise and detector (shot/electronic) noise. Laser-source noise, driven by pump instability and thermal drift [59], typically governs classical interferometry, whereas detection noise [60] prevails in low-photon quantum regimes. Existing techniques fail to address these distinct yet pervasive noise mechanisms simultaneously.

Here, we validate AWVA’s universal advantage over standard WVA under realistic noise conditions. Through analytical modeling and controlled Simulink simulations, we demonstrate AWVA’s dual capability: it suppresses both high-power laser noise and photon-starved detec-

* Contact author: xyhu@cug.edu.cn

† Contact author: jinghuihuang@cug.edu.cn

‡ Contact author: Adetunmise.Dada@glasgow.ac.uk

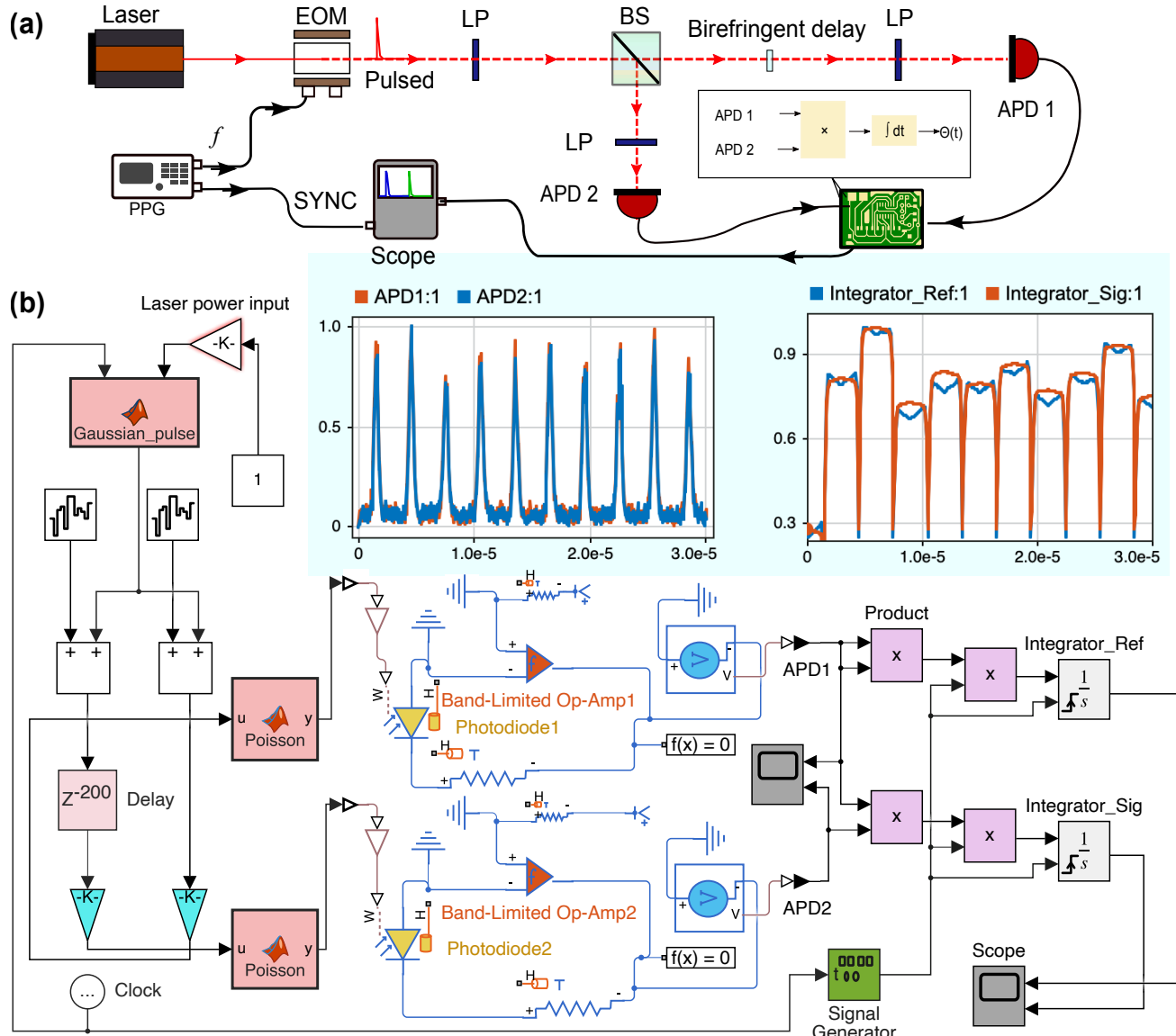


FIG. 1. **Weak-value amplification for birefringent time-delay measurement under realistic noise.** (a) AWVA experimental setup. A Gaussian pulse generated by a laser-EOM pair driven by a programmable pulse generator (PPG) is linearly polarised at 45° . A beam splitter (BS) creates two paths. Path 1 acquires a weak birefringent delay, is post-selected by a polariser at $(\alpha - 45^\circ)$, and is detected by APD1. Path 2, with the same polariser angle, serves as a reference detected by APD2. The two photodiode outputs are multiplied and integrated to obtain $\Theta(t)$. (b) Simulink model schematic showing band-limited laser noise N_s added at the source and detector noise N_d (shot + electronic) added at each APD. The Simulink model is available in Ref. [53].

tion noise while approaching the CRB in detection-noise-limited scenarios. Crucially, AWVA achieves this without prior knowledge of noise spectra or secondary filtering—a key advance for real-time sensing. By unifying noise-robust correlation strategies across classical and quantum domains, our results establish AWVA as a versatile tool for optical gyroscopes, gravitational-wave detection, and quantum sensing.

II. THE AWVA PROTOCOL ON SIMULINK

Fig. 1(a) illustrates the AWVA protocol setup [54] for measuring a birefringent delay. In contrast, standard WVA (described in Ref. [61]) omits the 50:50 beam splitter and reference arm. The key difference is that AWVA adds an extra light path (reference arm) parallel to the measurement arm, enabling an auto-correlation of outputs. The AWVA technique includes an initial preparation of the measured system $|\Phi_i\rangle$ and the pointer $|\Psi_i\rangle$,

followed by a weak interaction between the two. The system is then post-selected via projection onto the state $|\Phi_f\rangle$, and the pointer is projectively measured to yield $|\Psi_{f1}\rangle$. A second, identical projective measurement is applied to the pointer state $|\Psi_{f2}\rangle$ obtained without the weak interaction. Finally, the auto-correlative intensity Θ is evaluated from the two outcomes $|\langle\Phi_{f1}|\Phi_i\rangle|^2$ and $|\langle\Phi_{f2}|\Phi_i\rangle|^2$.

The initial pointer with the Gaussian profile is prepared in the time domain:

$$\begin{aligned} I^{in}(t) &= P^{in} |\langle t|\Psi_i\rangle|^2 \\ &= P^{in} \frac{1}{(2\pi\zeta^2)^{1/4}} e^{-(t-t_0)^2/4\zeta^2}. \end{aligned} \quad (1)$$

where P^{in} represents the pulse amplitude (units of W), and ζ is the pointer spread. Then, the system and the pointer are weakly coupled with the interaction $\hat{H} = \tau\hat{A} \otimes \hat{p}$. The observable operator satisfies $\hat{A} = |H\rangle\langle H| - |V\rangle\langle V|$, and \hat{p} is the momentum operator conjugate to the position operator \hat{q} [11, 12, 16, 35]. Here, $|H\rangle$ and $|V\rangle$ represent the horizontally and vertically polarized states, respectively. In the standard WVA protocol, the final state of the pointer in the measurement channel is given by:

$$\begin{aligned} |\Psi_{f1}\rangle &= \langle\Phi_f| e^{-i\tau\hat{A}\otimes\hat{p}} |\Psi_i\rangle |\Phi_i\rangle \\ &\approx \langle\Phi_f| \left[1 - i\tau\hat{A} \otimes \hat{p}\right] |\Psi_i\rangle |\Phi_i\rangle \\ &= \langle\Phi_f| \Phi_i\rangle e^{-i\tau A_w \hat{p}} |\Psi_i\rangle, \end{aligned} \quad (2)$$

where $A_w := \langle\Phi_f| \hat{A} |\Phi_i\rangle / \langle\Phi_f|\Phi_i\rangle$ is the so-called weak value [11]. Note that the approximation in Eq. (2) only holds in the weak-measurement region, where the time shift τ is much smaller than the pointer spread ζ (see values in Table I). In this paper, the time shift τ in the position of the pointer is amplified by the real part of A_w : $\Delta\langle\hat{q}\rangle = \tau\text{Re}[A_w]$ [62]. To amplify τ , the system is pre- and post-selected into the states:

$$|\Phi_i\rangle = \sin\left(\frac{\pi}{4}\right) |H\rangle + \cos\left(\frac{\pi}{4}\right) |V\rangle, \quad (3)$$

$$|\Phi_f\rangle = \sin\left(-\frac{\pi}{4} + \alpha\right) |H\rangle + \cos\left(-\frac{\pi}{4} + \alpha\right) |V\rangle, \quad (4)$$

where α is the postselection angle. One then obtains the weak value as: $A_w = -\cot\alpha$, and the corresponding time shift τ can be obtained from the peak shift $\delta t = |\tau\text{Re}A_w| = \tau\cot\alpha$ of the signal detected by an Amplified photodiode (APD1), with the detected signal I_1^{out} calculated from Eq. (2) as:

$$\begin{aligned} I_1^{out}(t; \tau) &= P^{in} |\langle\Phi_f|\Phi_i\rangle|^2 e^{-2i\tau A_w \hat{p}} |\langle q|\Psi_i\rangle|^2 \\ &\approx \frac{P^{in}}{2} \frac{(\sin\alpha)^2}{(2\pi\zeta^2)^{1/4}} e^{-(t-t_0-\delta t)^2/4\zeta^2}. \end{aligned} \quad (5)$$

In the AWVA protocol, for the measurement in the reference channel without the weak interaction, the signal

detected by APD2 can be calculated by

$$\begin{aligned} I_2^{out}(t; \tau = 0) &= P^{in} |\langle\Phi_f|\Phi_i\rangle|^2 |\langle q|\Psi_i\rangle|^2 \\ &\approx \frac{P^{in}}{2} \frac{(\sin\alpha)^2}{(2\pi\zeta^2)^{1/4}} e^{-(t-t_0)^2/4\zeta^2}. \end{aligned} \quad (6)$$

Following the previous work [54], $\Theta(\tau)$ is defined as

$$\Theta(t; \tau) = \int_0^t I_1^{out}(t'; \tau) \times I_2^{out}(t') dt'. \quad (7)$$

In the previous work [54], we simulated the AWVA measurements under Gaussian noises with a simple assumption that the effect from all sources of noise is equivalent to adding a certain type of noise on APDs. Where the noises were assumed to be added directly to the final measured signal $I_1^{out}(t; \tau)$ at APD1 and $I_2^{out}(t; \tau)$ at APD2. While effective for benchmarking, this approach conflates the distinct physical origins and spectral profiles of laser source noise and detection noise—a simplification that limits applicability to real-world quantum metrology. Thus, we rigorously separate laser source noise and detection noise in the measurement chain (Fig. 1b). By modeling these noise regimes in Simulink, we will demonstrate AWVA’s ability to suppress both laser source noise and detection noise.

III. SIMULATION AND RESULTS

We quantify the precision of WVA and AWVA under dominant noise regimes using a Simulink model (Fig. 1b). Two noise sources are explicitly modeled: **Band-limited laser source noise** (N_s), added to the signal path with power P_s ; **Detection noise**, modeled as Poisson-distributed pre-detection photon-counting noise (shot noise), and electrical noise generated via photodiode and Op-Amp components to mimic electronic readout noise. In Fig. 1, shot noise is modeled via a function block implementing Matlab’s `poissrnd()` with incident power as input, while electrical noise is characterized by the parameters in Table I.

Precision is characterized by the standard deviation (Std) of the time-delay estimation for the WVA protocol (σ_1), the AWVA protocol (σ_2), and the Cramér-Rao bound (σ_3). For AWVA, σ_2 derives from the peak change in $\Theta(t; \tau)$, while σ_1 for WVA uses intensity centroid shifts. The CRB σ_3 sets the theoretical quantum limit [49]. In this paper, we define

$$\sigma_1 = \frac{\text{Std}[\text{Loc}(I_1^{out}(t; \tau)) - \text{Loc}(I_2^{out}(t; 0\text{s}))]}{\langle \text{Loc}(I_1^{out}(t; \tau)) - \text{Loc}(I_2^{out}(t; 0\text{s})) \rangle} \times \tau, \quad (8)$$

$$\sigma_2 = \frac{\text{Std}[\text{Peak}(\Theta(t; \tau)) - \text{Peak}(\Theta(t; 0\text{s}))]}{\langle \text{Peak}(\Theta(t; \tau)) - \text{Peak}(\Theta(t; 0\text{s})) \rangle} \times \tau, \quad (9)$$

$$\sigma_3^{-2} = \mathcal{N} \int_0^T I^{in}(t - \tau) \left[\frac{\partial}{\partial \tau} \ln I^{in}(t - \tau) \right]^2 dt, \quad (10)$$

where T is the pulse period, c is the speed of light, λ is the wavelength of the photons, $\mathcal{N} = \mathcal{G}P^{in}T\lambda/\hbar c$ is the total number of input photons, and $\mathcal{G} = 0.93$ is the correction factor for the Gaussian pulse. In this work, the CRB band is calculated, including shot noise (fundamental quantum noise) but excluding electronic readout noise with the approximation of the large- N limit. The function `Loc()` returns the temporal centroid (first moment) of $I_1^{out}(t; \tau)$, and the function `Peak()` returns the maximum (peak value) of $\Theta(t; \tau)$. In this work, we investigate two different scenarios where laser-source noise or detection noise dominates.

To ensure a fair comparison between the WVA and AWVA techniques, which use different observables (the intensity profile $I(t)$ and the autocorrelation $\Theta(t)$, respectively), we define the estimation precision for the time delay τ itself. For any unbiased estimator y that is linearly proportional to τ (i.e., $\langle y \rangle = k\tau$), the standard deviation of the estimated τ is given by:

$$\text{Std}[\tau] = \frac{\text{Std}[y]}{k}. \quad (11)$$

The quantity $\text{Std}[\tau]$ is a figure of merit for the estimation error that is independent of the specific choice of estimator y . For the WVA technique, we use $y = \text{Loc}(I_1^{out}(t; \tau)) - \text{Loc}(I_2^{out}(t; 0\text{s}))$ and calculate $k = |d\langle I(t) \rangle/d\tau|$ around the operating point. This leads directly to the definition of σ_1 in Eq. (8). Similarly, for the AWVA technique, we use $y = \text{Peak}(\Theta(t; \tau)) - \text{Peak}(\Theta(t; 0\text{s}))$ and its corresponding slope to define σ_2 in

TABLE I. Simulation parameters in Simulink. Scenario I and Scenario II are simulated with the same parameters, except $P_s(\text{S. I})$ and $P_s(\text{S. II})$ of the laser noise power. Note that the detection noise N_d , including the shot noise and electrical noise, can not be quantified, since the amplitude of N_d depends on the signal.

Type	Parameter	Meaning	Value
WVA	τ	Birefringent delay	1×10^{-10} s
	α	Postselection angle	0.01 rad
	$\text{Re}A_w$	Weak value	100
	λ	Wavelength	633 nm
Laser	P^{in}	Amplitude	10^{-3} - 10^4 W
	$P_s(\text{S. I})$	Noise power	2×10^{-14} W 2 /Hz
	$P_s(\text{S. II})$	Noise power	2×10^{-22} W 2 /Hz
	ζ	Spread	2×10^{-7} s
Detection	T	Pulse period	3×10^{-6} s
	t_0	Time offset for pulse	1.5×10^{-6} s
	$1/f_d$	Sample time	5×10^{-11} s
	S_d	Sensitivity	113×10^{-10} Am 2 /W
	I_d	Dark current	1×10^{-6} A
	A_d	Gain	10000
	f_d	Bandwidth	2×10^{10} Hz

Eq. (9). Consequently, both σ_1 and σ_2 represent $\text{Std}[\tau]$, allowing for their direct comparison.

Scenario I (Laser noise dominates): Set high-power laser and larger laser source noise N_s . We show the power spectral density (PSD) results of three simulations for the WVA protocol in Fig. 2(a), including different signal combinations of the ideal signal input (S), the laser source noise N_s and the detection noise N_d . When setting $P^{in} = 100$ mW, the curve $\text{PSD}(S+N_d)$ is much lower than the curves $\text{PSD}(S+N_s+N_d)$ and $\text{PSD}(N_s+N_d)$, indicating that N_d contributes little to the final signal $I_1^{out}(t; \tau)$ thus the laser source noise dominates.

Scenario II (Detection noise dominates): Set low-power laser and smaller laser source noise N_s . Similarly, the PSD curves with setting $P^{in} = 0.01$ mW are present in Fig. 2(c). In contrast to Scenario I, the curve $\text{PSD}(S+N_d)$ almost overlaps with the curve $\text{PSD}(S+N_s+N_d)$, indicating that N_s contributes little to the final signal $I_1^{out}(t; \tau)$, thus the detection noise dominates.

Our numerical experiments quantify AWVA's advantage across two noise-dominated regimes. For each input pulse amplitude P^{in} , we simulated 100 independent measurements of time delay $\tau = 0.1$ ns over $t_{stop} = 3 \times 10^{-4}$ s. We represent the main simulation parameters in Table I and code in Ref. [53]. Figure 2(b) and (d) compare AWVA and WVA performance in Scenario I (laser noise-dominated) and Scenario II (detection noise-limited), respectively. It can be found that the statistical standard deviation σ_2 of the AWVA measurement is smaller than σ_1 of the WVA measurement, despite the laser input power. At $P_{in} = 0.01$ mW (Scenario II), WVA yields $\sigma_1 \approx 0.3$ ns whereas AWVA yields $\sigma_2 \approx 0.03$ ns (Fig. 2(d)), nearly 10 \times improvement.

In Scenario I, the noise-reduction advantages of AWVA over WVA will be highlighted when increasing the input laser power. AWVA's σ_2 is 10% lower than σ_1 at the highest powers (Fig. 2(b)). In addition, Fig. 2(d) for Scenario II shows that precision in AWVA is improved by approximately one order of magnitude of std compared to WVA, demonstrating the ability to approach the CRB limit.

IV. DISCUSSION AND SUMMARY

In Scenario I, AWVA reduces the statistical uncertainty σ_2 by up to 10% compared to WVA's σ_1 at high laser power $P^{in} > 100$ mW, where laser power fluctuations dominate (Fig. 2(b)). This scaling arises because AWVA's auto-correlative post-processing suppresses laser noise, which grows with input power. In contrast, WVA's single-shot measurements fail to leverage these correlations, leaving it susceptible to noise amplification at elevated powers—a critical drawback in high-power interferometric systems.

Scenario II highlights AWVA's quantum advantage: under detection noise (shot and amplifier noise), AWVA

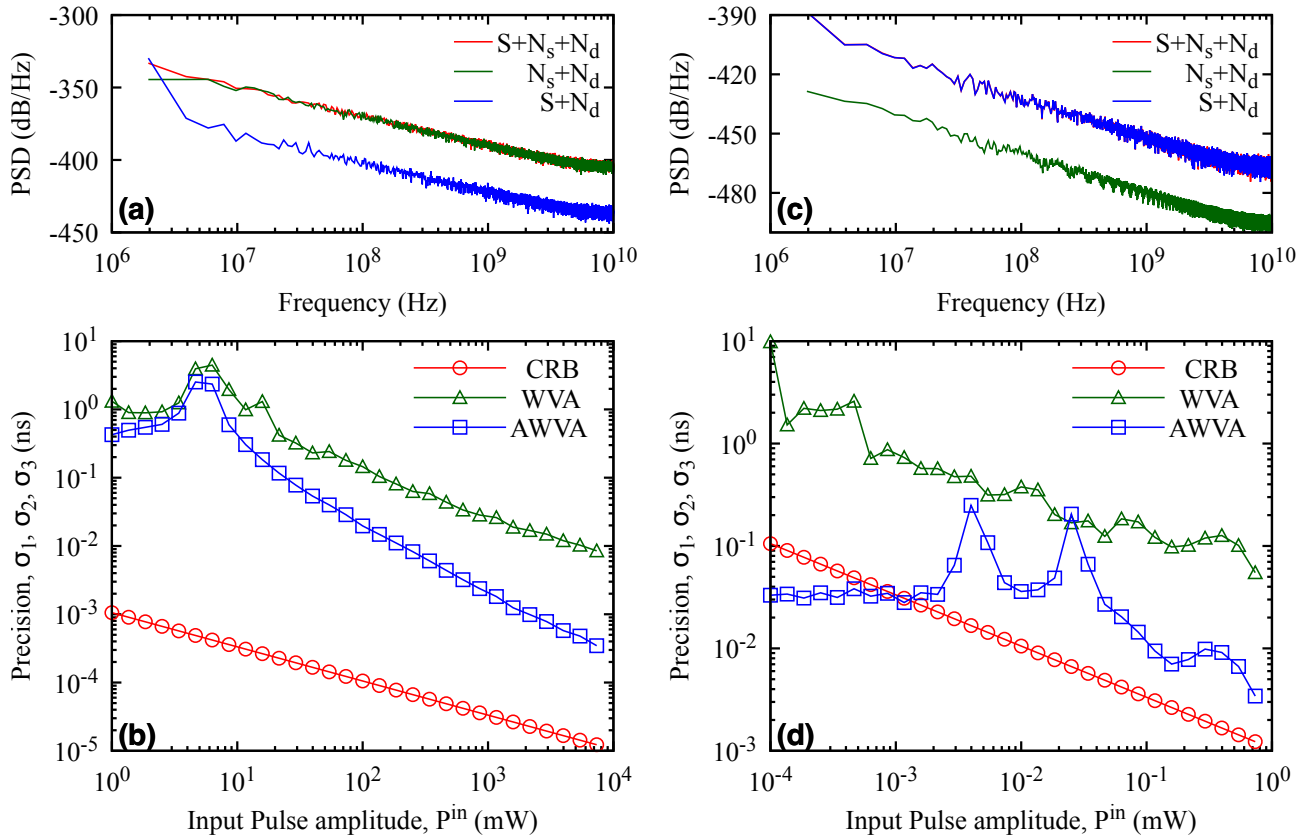


FIG. 2. **Simulated time delay measurement performance of WVA and AWVA protocols.** The value of the time delay is set at $\tau = 0.1$ ns. (a) Power spectral density (PSD) of WVA signals in Scenario I (high-power laser, $P^{in} = 100$ mW). Laser source noise N_s dominates over detection noise N_d . Here, the labels “ $S+N_s+N_d$ ”, “ $S+N_d$ ”, and “ N_s+N_d ” denote distinct combinations of the ideal signal (S), laser source noise (N_s), and detection noise (N_d). (b) Time delay estimation precision of the WVA, AWVA, and Cramér-Rao bound (CRB) limits for Scenario I. Here, the CRB bound is calculated based on the formula (10). (c) PSD results for Scenario II (low-power, $P^{in} = 0.01$ mW). (d) Time delay estimation precision of the WVA, AWVA, and CRB limits for Scenario II.

achieves a remarkable reduction in σ_2 over WVA, closely approaching the CRB (Fig. 2(d)). This aligns with our analytical models, where AWVA’s correlated sampling cancels detection-stage noise correlations, enabling sub-shot-noise sensitivity. The CRB proximity confirms AWVA’s superiority in photon-limited regimes, overcoming WVA’s trade-off between amplification and noise susceptibility.

The sub-CRB precision in Fig. 2(d) (low input-amplitude regime) arises from finite sampling effects and a benchmark mismatch, not a physical surpassing of the fundamental limit. The CRB is an asymptotic limit for unbiased estimators under a specified noise model. Our precision points in Fig. 2 are computed from $N = 100$ Monte-Carlo trials, making it possible for the resulting finite-sample RMSE to fluctuate slightly below the asymptotic CRB at low input powers. Importantly, our CRB curve assumes an ideal broadband detector, whereas the Simulink model includes a band-limited, slew-rate-limited amplifier with mild nonlinearities, which reshape the noise spectrum. While electronics add noise overall, such filtering can reduce the variance

captured by our estimator relative to an idealized CRB. For Fisher information computed with the detector’s actual transfer function and noise PSD, the bound would shift accordingly and the apparent sub-CRB dip disappears. Thus, no fundamental limit is violated.

In addition, the pronounced oscillations of curves $\sigma_1(P^{in})$ and $\sigma_2(P^{in})$ in Scenario II arise from finite simulation time $t_{stop} = 3 \times 10^{-4}$ and the stochastic nature of detection noise. While longer simulations would smooth these artifacts, computational constraints limit practical runtime due to the model’s complexity. Nonetheless, our Simulink framework—employing engineering-grade parameters—provides a scalable platform to study detection noise, bridging the gap between idealized theory [37, 55–58] and real-world optoelectronic systems.

In summary, we demonstrate that AWVA universally enhances phase estimation under realistic non-Gaussian noise. Our numerical model confirms that AWVA outperforms WVA under both dominant laser noise and dominant detector noise. These results unify AWVA’s utility across classical and quantum sensing paradigms. By suppressing both laser noise and detection noise with-

out prior spectral knowledge, AWVA demonstrates the ability to approach the CRB limit in detection-noise-limited scenarios. This dual capability is critical for hybrid systems, such as optomechanical sensors or gyroscopes, where noise sources coexist [63, 64]. Furthermore, AWVA’s computational simplicity—requiring only post-measurement correlation—enables real-time operation, which can be implemented in an FPGA-based [65] high-speed optical sensor. While these results are based on simulation, they suggest AWVA could be implemented in real sensors to enhance precision. Our results establish AWVA as a versatile strategy for applications that demand both high-power interferometry and photon-starved quantum sensing, thereby unifying classical and quantum noise resilience under a single protocol.

ACKNOWLEDGMENTS

This study was supported by the National Natural Science Foundation of China (Grants No. 42327803,

No. 42504048, and No. 42488201). J-H. Huang acknowledges support from the Hubei Provincial Natural Science Foundation of China (Grant No. 20250650025), the Fellowship Program of China National Postdoctoral Program for Innovative Talents under Grant Number BX20250161, and the CSC. A.C.D. acknowledges support from the EPSRC, Impact Acceleration Account (Grant No. EP/R511705/1).

Data availability—The data that support the findings of this paper are openly available [53].

[1] K. Pawłowski, D. Spehner, A. Minguzzi, and G. Ferrini, Macroscopic superpositions in bose-josephson junctions: Controlling decoherence due to atom losses, *Phys. Rev. A* **88**, 013606 (2013).

[2] P. Szañkowski, G. Ramon, J. Krzywda, D. Kwiatkowski, and L. Cywiński, Environmental noise spectroscopy with qubits subjected to dynamical decoupling, *J. Phys.:Condens. Matter* **29**, 333001 (2017).

[3] F.-Y. Ma, J.-G. Li, and J. Zou, The influence of non-gaussian noise on weak values, *Physics Letters A* **388**, 127027 (2021).

[4] M. Abe and M. Ban, Decoherence of a weak value influenced by a non-Markovian environment, *Quantum Studies: Mathematics and Foundations* **3**, 313 (2016).

[5] M. Ban, Weak measurement on a quantum system in contact with a thermal reservoir: projection operator method, *Quantum Studies: Mathematics and Foundations* **4**, 339 (2017).

[6] B. P. A. et al, Characterization of transient noise in advanced LIGO relevant to gravitational wave signal GW150914, *Classical and Quantum Gravity* **33**, 134001 (2016).

[7] N. J. Cornish, T. B. Littenberg, B. Bécsy, K. Chatziioannou, J. A. Clark, S. Ghonge, and M. Millhouse, Bayeswave analysis pipeline in the era of gravitational wave observations, *Phys. Rev. D* **103**, 044006 (2021).

[8] N. J. Cornish and T. B. Littenberg, Bayeswave: Bayesian inference for gravitational wave bursts and instrument glitches, *Classical and Quantum Gravity* **32**, 135012 (2015).

[9] J. Y. L. Kwok, R. K. L. Lo, A. J. Weinstein, and T. G. F. Li, Investigation of the effects of non-gaussian noise transients and their mitigation in parameterized gravitational-wave tests of general relativity, *Phys. Rev. D* **105**, 024066 (2022).

[10] B. Zackay, T. Venumadhav, J. Roulet, L. Dai, and M. Zaldarriaga, Detecting gravitational waves in data with non-stationary and non-gaussian noise, *Phys. Rev. D* **104**, 063034 (2021).

[11] Y. Aharonov, D. Z. Albert, and L. Vaidman, How the result of a measurement of a component of the spin of a spin-1/2 particle can turn out to be 100, *Phys. Rev. Lett.* **60**, 1351 (1988).

[12] J. Dressel, M. Malik, F. M. Miatto, A. N. Jordan, and R. W. Boyd, Colloquium: Understanding quantum weak values: Basics and applications, *Rev. Mod. Phys.* **86**, 307 (2014).

[13] J. Ren, L. Qin, W. Feng, and X.-Q. Li, Weak-value-amplification analysis beyond the aharonov-albert-vaidman limit, *Phys. Rev. A* **102**, 042601 (2020).

[14] P. Yin, W.-H. Zhang, L. Xu, Z.-G. Liu, W.-F. Zhuang, L. Chen, M. Gong, Y. Ma, X.-X. Peng, G.-C. Li, J.-S. Xu, Z.-Q. Zhou, L. Zhang, G. Chen, C.-F. Li, and G.-C. Guo, Improving the precision of optical metrology by detecting fewer photons with biased weak measurement, *Light: Sci. Appl.* **10**, 103 (2021).

[15] F. Lecocq, L. Ranzani, G. A. Peterson, K. Cicak, X. Y. Jin, R. W. Simmonds, J. D. Teufel, and J. Aumentado, Efficient qubit measurement with a nonreciprocal microwave amplifier, *Phys. Rev. Lett.* **126**, 020502 (2021).

[16] C. Krafczyk, A. N. Jordan, M. E. Goggin, and P. G. Kwiat, Enhanced weak-value amplification via photon recycling, *Phys. Rev. Lett.* **126**, 220801 (2021).

[17] J. T. Monroe, N. Yunger Halpern, T. Lee, and K. W. Murch, Weak measurement of a superconducting qubit reconciles incompatible operators, *Phys. Rev. Lett.* **126**, 100403 (2021).

[18] B. Xia, J. Huang, H. Li, H. Wang, and G. Zeng, Toward incompatible quantum limits on multiparameter estimation, *Nat. Commun.* **14**, 1021 (2023).

[19] R. Dhara, N. Modak, S. Guchhait, and N. Ghosh, Roadmap on weak measurements in optics, *Advanced*

Physics Research **n/a**, 2400136.

[20] Y. Makhlin, G. Schön, and A. Shnirman, Quantum-state engineering with josephson-junction devices, *Rev. Mod. Phys.* **73**, 357 (2001).

[21] P. B. Dixon, D. J. Starling, A. N. Jordan, and J. C. Howell, Ultrasensitive beam deflection measurement via interferometric weak value amplification, *Phys. Rev. Lett.* **102**, 173601 (2009).

[22] G. I. Viza, J. Martínez-Rincón, G. A. Howland, H. Frostig, I. Shomroni, B. Dayan, and J. C. Howell, Weak-values technique for velocity measurements, *Opt. Lett.* **38**, 2949 (2013).

[23] J.-H. Huang, F.-F. He, X.-Y. Duan, G.-J. Wang, and X.-Y. Hu, Modified weak-value-amplification technique for measuring a mirror's velocity based on the vernier effect, *Phys. Rev. A* **105**, 013718 (2022).

[24] B. de Lima Bernardo, S. Azevedo, and A. Rosas, Ultra-small polarization rotation measurements via weak value amplification, *Physics Letters A* **378**, 2029 (2014).

[25] O. S. Magaña Loaiza, M. Mirhosseini, B. Rodenburg, and R. W. Boyd, Amplification of angular rotations using weak measurements, *Phys. Rev. Lett.* **112**, 200401 (2014).

[26] A. Feizpour, X. Xing, and A. M. Steinberg, Amplifying single-photon nonlinearity using weak measurements, *Phys. Rev. Lett.* **107**, 133603 (2011).

[27] M. Hallaji, A. Feizpour, G. Dmochowski, J. Sinclair, and A. M. Steinberg, Weak-value amplification of the nonlinear effect of a single photon, *Nat. Phys.* **13**, 540 (2017).

[28] H. Li, J.-Z. Huang, Y. Yu, Y. Li, C. Fang, and G. Zeng, High-precision temperature measurement based on weak measurement using nematic liquid crystals, *Applied Physics Letters* **112**, 231901 (2018).

[29] Y. Li, H. Li, J. Huang, C. Fang, M. Liu, C. Huang, and G. Zeng, High-precision temperature sensor based on weak measurement, *Opt. Express* **27**, 21455 (2019).

[30] J.-H. Huang, X.-Y. Duan, G.-J. Wang, and X.-Y. Hu, Enhancing the precision of detecting weak magnetic fields based on weak-value amplification, *J. Opt. Soc. Am. B* **39**, 1289 (2022).

[31] O. Hosten and P. Kwiat, Observation of the spin hall effect of light via weak measurements, *Science* **319**, 787 (2008).

[32] H. Luo, X. Zhou, W. Shu, S. Wen, and D. Fan, Enhanced and switchable spin hall effect of light near the brewster angle on reflection, *Phys. Rev. A* **84**, 043806 (2011).

[33] S. Chen, X. Ling, W. Shu, H. Luo, and S. Wen, Precision measurement of the optical conductivity of atomically thin crystals via the photonic spin hall effect, *Phys. Rev. Appl.* **13**, 014057 (2020).

[34] T. Li, Y. Wang, Y. Jiang, S. Zhang, L. Luo, and Z. Zhang, High-precision measurement of the complex magnetooptical kerr effect using weak measurement, *Appl. Phys. Lett.* **124**, 054001 (2024).

[35] X.-Y. Xu, Y. Kedem, K. Sun, L. Vaidman, C.-F. Li, and G.-C. Guo, Phase estimation with weak measurement using a white light source, *Phys. Rev. Lett.* **111**, 033604 (2013).

[36] Y. Yang, Y. Xu, T. Guan, L. Shi, J. Li, D. Li, Y. He, X. Wang, Z. Li, and Y. Ji, Spectrum intensity ratio detection for frequency domain weak measurement system, *IEEE Photonics Journal* **12**, 1 (2020).

[37] A. N. Jordan, J. Martínez-Rincón, and J. C. Howell, Technical advantages for weak-value amplification: When less is more, *Phys. Rev. X* **4**, 011031 (2014).

[38] D. J. Starling, P. B. Dixon, A. N. Jordan, and J. C. Howell, Optimizing the signal-to-noise ratio of a beam-deflection measurement with interferometric weak values, *Phys. Rev. A* **80**, 041803 (2009).

[39] N. Modak, A. B S, A. K. Singh, and N. Ghosh, Generalized framework of weak-value amplification in path interference of polarized light for the enhancement of all possible polarization anisotropy effects, *Phys. Rev. A* **103**, 053518 (2021).

[40] J. Harris, R. W. Boyd, and J. S. Lundeen, Weak value amplification can outperform conventional measurement in the presence of detector saturation, *Phys. Rev. Lett.* **118**, 070802 (2017).

[41] J. Martínez-Rincón, W.-T. Liu, G. I. Viza, and J. C. Howell, Can anomalous amplification be attained without postselection?, *Phys. Rev. Lett.* **116**, 100803 (2016).

[42] M. Song, J. Steinmetz, Y. Zhang, J. Nauriyal, K. Lyons, A. N. Jordan, and J. Cardenas, Enhanced on-chip phase measurement by inverse weak value amplification, *Nat. Commun.* **12**, 6247 (2021).

[43] Y. Kim, S.-Y. Yoo, and Y.-H. Kim, Heisenberg-limited metrology via weak-value amplification without using entangled resources, *Phys. Rev. Lett.* **128**, 040503 (2022).

[44] Y. Wang, W. Zhang, S. Chen, S. Wen, and H. Luo, Multiple-weak-value quantum measurement for precision estimation of time delay, *Phys. Rev. A* **105**, 033521 (2022).

[45] J.-Z. Huang, C. Fang, and G. Zeng, Weak-value-amplification metrology without spectral analysis, *Phys. Rev. A* **97**, 063853 (2018).

[46] Z.-P. Li, Y.-T. Wang, S. Yu, W. Liu, Y. Meng, Y.-Z. Yang, Z.-A. Wang, N.-J. Guo, X.-D. Zeng, J.-S. Tang, C.-F. Li, and G.-C. Guo, Experimental investigation of high-efficiency weak-value amplification of nonunitary evolution, *Phys. Rev. A* **106**, 012608 (2022).

[47] X. Tan, H. Li, Q. Song, C. Shi, Q. Deng, B. Xia, Z. Luo, J. Huang, and G. Zeng, Noise mitigation for high-sensitivity phase estimation based on weak measurements, *Phys. Rev. A* **109**, 053512 (2024).

[48] J.-H. Huang, K. M. Jordan, A. C. Dada, X.-Y. Hu, and J. S. Lundeen, Enhancing interferometry using weak value amplification with real weak values, *Phys. Rev. Lett.* **134**, 080802 (2025).

[49] S. Pang and T. A. Brun, Improving the precision of weak measurements by postselection measurement, *Phys. Rev. Lett.* **115**, 120401 (2015).

[50] G. C. Knee and E. M. Gauger, When amplification with weak values fails to suppress technical noise, *Phys. Rev. X* **4**, 011032 (2014).

[51] Y. Liu, L. Qin, and X.-Q. Li, Fisher information analysis on weak-value-amplification metrology using optical coherent states, *Phys. Rev. A* **106**, 022619 (2022).

[52] M. Zhang, J. Zhang, C. Wu, Y. Xie, T. Chen, W. Wu, and P. Chen, Optimization of parameter measurement precision with precoupling-assisted weak-value amplification, *Phys. Rev. A* **107**, 042601 (2023).

[53] J.-H. Huang, Code for: Mitigating Source and Detection Noises in Auto-correlative Weak-Value Amplification (2025), harvard Dataverse, V1.

[54] J.-H. Huang, X.-Y. Hu, A. C. Dada, J. S. Lundeen, K. M. Jordan, H. Chen, and J. An, Autocorrelative weak-value amplification and simulating the protocol under strong gaussian noise, *Phys. Rev. A* **106**, 053704 (2022).

[55] R. F. Fox, I. R. Gatland, R. Roy, and G. Vemuri, Fast, accurate algorithm for numerical simulation of exponentially correlated colored noise, *Phys. Rev. A* **38**, 5938 (1988).

[56] B. L. Hu, J. P. Paz, and Y. Zhang, Quantum brownian motion in a general environment: Exact master equation with nonlocal dissipation and colored noise, *Phys. Rev. D* **45**, 2843 (1992).

[57] J.-L. Wu, W.-L. Duan, Y. Luo, and F. Yang, Time delay and non-gaussian noise-enhanced stability of foraging colony system, *Phys. A* **553**, 124253 (2020).

[58] O. V. Pountougnigni, R. Yamapi, C. Tchawoua, V. Pierro, and G. Filatrella, Detection of signals in presence of noise through josephson junction switching currents, *Phys. Rev. E* **101**, 052205 (2020).

[59] J. Kim and Y. Song, Ultralow-noise mode-locked fiber lasers and frequency combs: principles, status, and applications, *Adv. Opt. Photon.* **8**, 465 (2016).

[60] Y. Xiang, H. Cao, C. Liu, J. Guo, and D. Dai, High-speed waveguide ge/si avalanche photodiode with a gain-bandwidth product of 615 ghz, *Optica* **9**, 762 (2022).

[61] N. Brunner and C. Simon, Measuring small longitudinal phase shifts: Weak measurements or standard interferometry?, *Phys. Rev. Lett.* **105**, 010405 (2010).

[62] Y. Susa, Y. Shikano, and A. Hosoya, Optimal probe wave function of weak-value amplification, *Phys. Rev. A* **85**, 052110 (2012).

[63] S. Zhao, Q. Liu, Y. Liu, H. Ma, and Z. He, Navigation-grade resonant fiber-optic gyroscope using ultra-simple white-light multibeam interferometry, *Photon. Res.* **10**, 542 (2022).

[64] Y. Liu, Y. Zhang, Z. Xu, L. Zhou, Y. Zou, B. Zhang, and Z. Hu, Ultra-low noise phase measurement of fiber optic sensors via weak value amplification, *Opt. Express* **30**, 18966 (2022).

[65] J. Elaskar, M. A. Luda, L. Tozzetti, J. Codnia, and C. J. Oton, Fpga-based high-speed optical fiber sensor based on multitone-mixing interferometry, *IEEE Trans. Instrum. Meas.* **71**, 1 (2022).